



Supplement of

Understanding the long-term trend of organic aerosol and the influences from anthropogenic emission and regional climate change in China

Wenxin Zhang et al.

Correspondence to: Xinyi Dong (dongxy@nju.edu.cn)

The copyright of individual parts of the supplement might differ from the article licence.

Text S1: Model evaluation supplement. In addition to evaluating OA and its sub-species, this study also assessed other relevant factors that play a critical role in understanding the processes driving OA formation and its atmospheric impacts. O₃ was closely related to production of SOA as it was involved in VOC-related chemistry. The model generally underestimated O₃ with a NMB of -17.9% compared to ground-based observations (Fig.S6(b)). Furthermore, since one of the pathways for the formation of SOA_{MT} involves reactions with the oxidant NO₂, we evaluated the model's simulation of NO₂ column density compared to satellite data, finding an NMB of 6.2% (Fig.S6(d)). In addition, as AOD is a crucial indicator of the total column burden of aerosols and plays an important role in understanding aerosol radiative effects, we also assessed the model's performance in simulating AOD (Fig.S6(c)), with an NMB of -41.4%. The model was found to be able to generally reproduce spatial distributions of these variables as well, with more details provided in Fig.S6. Simulation performance of CAM-Chem for O₃, NO₂ column density and AOD has been thoroughly discussed in recent publications (Emmons et al., 2020; Jo et al., 2021; Schwantes et al., 2020), and our results are in good agreement with these previous findings.

Text S2: Trend and attribution of Surface OA supplement. The annual variations of surface OA are presented by shaded areas representing contributions from POA and SOA as shown in Fig.S7(a). We find in the simulation that surface OA concentration increased by 5.6% (0.25 μg m⁻³) over 1990-2019 as a combined result of a decrease in POA by -0.24 μg m⁻³ (-8.1%) and an increase in SOA by 0.49 μg m⁻³ (32.3%). Over the study period, proportion of POA in total OA decreased from 69.4% to 59.1% as shown in Fig.S8(a). It should be noticed that the change in OA was non-monotonical over the whole study period. Total OA concentration gradually increased by 1.7% per year over 1990-2006 and decreased by -3.2% per year over 2007-2019. Fig.S7(a) implies that neither changes in POA or SOA were monotonical, which was closely related to the implementation of anthropogenic emission management policies in China. In addition, changes of OA and subspecies at different seasons (Fig.S11) suggested that annual variation in OA was mainly driven by POA, which varied greatly in spring and summer due to contributions from biomass burning (Fig.S13).

Text S3: In CAM6-Chem, SVOC emissions are parameterized as 60% of the POM emissions, while IVOC emissions are estimated as 20% of the non-methane VOC emissions (Tilmes et al., 2019). As shown in the formula below.

$$\text{IVOC} = 0.2 * (\text{C3H6} + \text{C3H8} + \text{C2H6} + \text{C2H4} + \text{BIGENE} + \text{BIGALK} + \text{CH3COCH3} + \text{MEK} + \text{CH3CHO} + \text{CH2O} + \text{BENZENE} + \text{TOLUENE} + \text{XYLENES}) \quad (\text{S1})$$

$$\text{SVOC} = 0.6 * \text{pom_a4} \quad (\text{S2})$$

Species	Chemical formula	Description
C3H6	C ₃ H ₆	propene
C3H8	C ₃ H ₈	propane

C2H6	C ₂ H ₆	ethane
C2H4	C ₂ H ₄	ethene
BIGENE	C ₄ H ₈	lumped alkenes C>3
BIGALK	C ₅ H ₁₂	lumped alkanes C>3
CH3COCH3	CH ₃ COCH ₃	acetone
MEK	C ₄ H ₈ O	methyl ethyl ketone
CH3CHO	CH ₃ CHO	acetaldehyde
CH2O	CH ₂ O	formaldehyde
BENZENE	C ₆ H ₆	benzene
TOLUENE	C ₇ H ₈	toluene
XYLENES	C ₈ H ₁₀	lumped xylenes
pom_a4	C	primary organic matter, MAM primary carbon mode

30 **Table S1. Species used for S/IVOC emission calculations.**

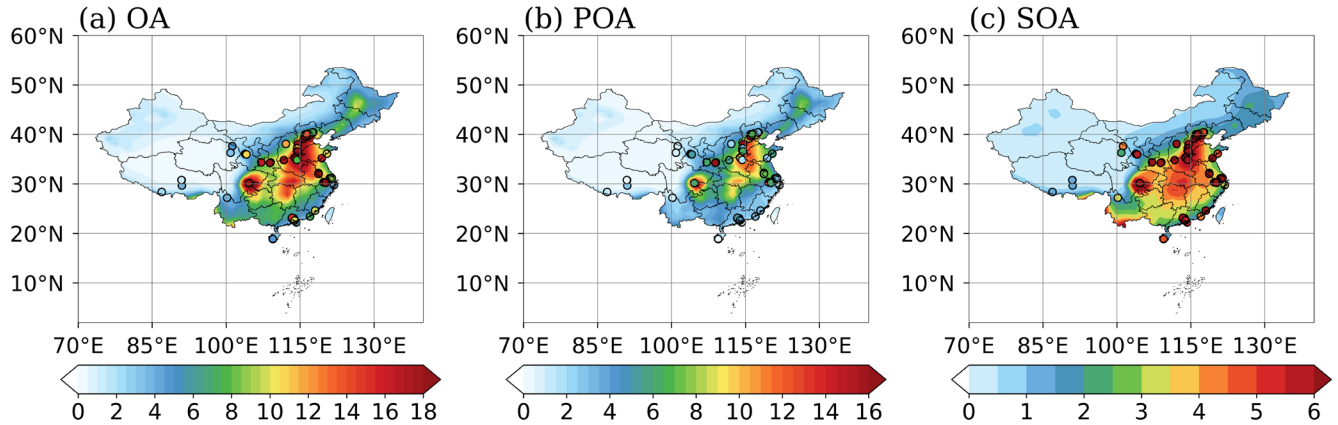
year	SOA ¹	SOA ²	POA ¹	POA ²	OA ¹	OA ²
1990	1.21	1.73	2.75	4.14	3.96	5.87
1991	1.22	1.73	2.75	4.14	3.98	5.87
1992	1.33	1.90	2.93	4.43	4.26	6.34
1993	1.21	1.72	2.72	4.09	3.94	5.80
1994	1.32	1.89	2.88	4.33	4.20	6.21
1995	1.26	1.79	2.85	4.27	4.11	6.06
1996	1.25	1.78	2.74	4.09	3.99	5.87
1997	1.38	1.97	2.94	4.39	4.32	6.36
1998	1.51	2.17	3.27	4.92	4.78	7.08
1999	1.26	1.78	2.75	4.08	4.01	5.85
2000	1.29	1.83	2.71	4.05	4.00	5.88

2001	1.31	1.87	2.76	4.12	4.07	5.99
2002	1.47	2.10	3.04	4.54	4.51	6.63
2003	1.77	2.58	3.90	5.89	5.67	8.47
2004	1.63	2.35	3.38	5.08	5.00	7.43
2005	1.56	2.24	3.19	4.79	4.75	7.03
2006	1.75	2.53	3.50	5.25	5.25	7.78
2007	1.80	2.62	3.48	5.25	5.28	7.87
2008	1.71	2.47	3.32	5.00	5.04	7.47
2009	1.77	2.54	3.31	4.93	5.07	7.48
2010	1.57	2.26	2.99	4.46	4.56	6.72
2011	1.73	2.52	3.23	4.85	4.96	7.37
2012	1.78	2.54	3.15	4.64	4.93	7.18
2013	1.86	2.72	3.19	4.77	5.05	7.49
2014	1.78	2.57	3.09	4.60	4.87	7.17
2015	1.70	2.45	2.76	4.10	4.46	6.55
2016	1.55	2.22	2.39	3.51	3.94	5.73
2017	1.45	2.07	2.23	3.28	3.68	5.35
2018	1.41	2.01	2.09	3.06	3.49	5.07
2019	1.49	2.13	2.14	3.16	3.63	5.29
multi-year arithmetic mean (ug/m ³)	1.51	2.17	2.95	4.41	4.46	6.58
Trend (ug/m ³ per year)	0.02	0.02	-0.01	-0.01	0.01	0.01

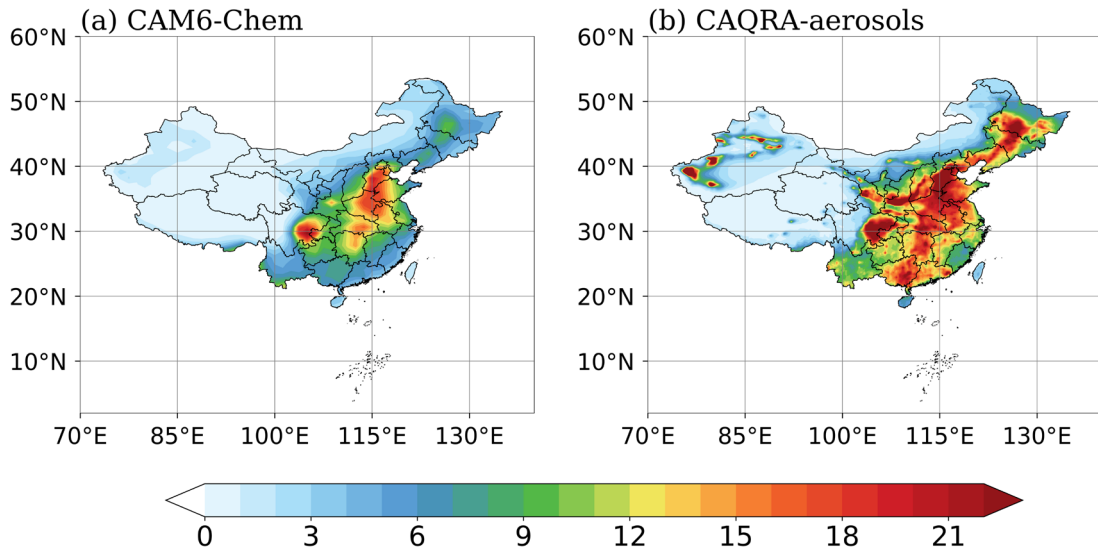
Trend (% per year)	1.08	1.12	-0.27	-0.32	0.19	0.15
--------------------	------	------	-------	-------	------	------

32 Table S2. Simulated annual average concentrations (units: $\mu\text{g}/\text{m}^3$) of surface OA, POA, and SOA from 1990 to 2019, along with their
 34 multi-year arithmetic mean (units: $\mu\text{g}/\text{m}^3$) and trends. Superscript 1 indicates the calculation for the regional average concentration
 values for China, while superscript 2 indicates the calculation for the regional average concentration values for China excluding
 Xinjiang, Tibet, and Qinghai.

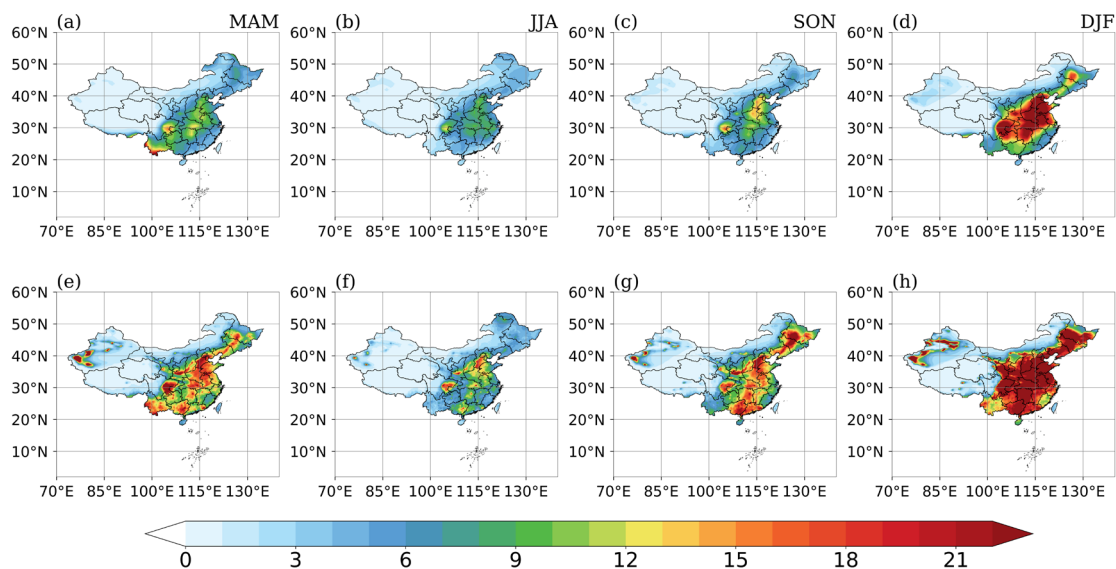
36



38 Figure S1. 2013 to 2019 annual average of surface organic aerosols (OA; a), primary organic aerosols (POA; b) and secondary
 40 organic aerosols (SOA; c) concentrations in our model and ground-based measurements (filled circles) compiled by Miao et al. (2021)
 and Chen et al. (2024) (unit: $\mu\text{g m}^{-3}$).



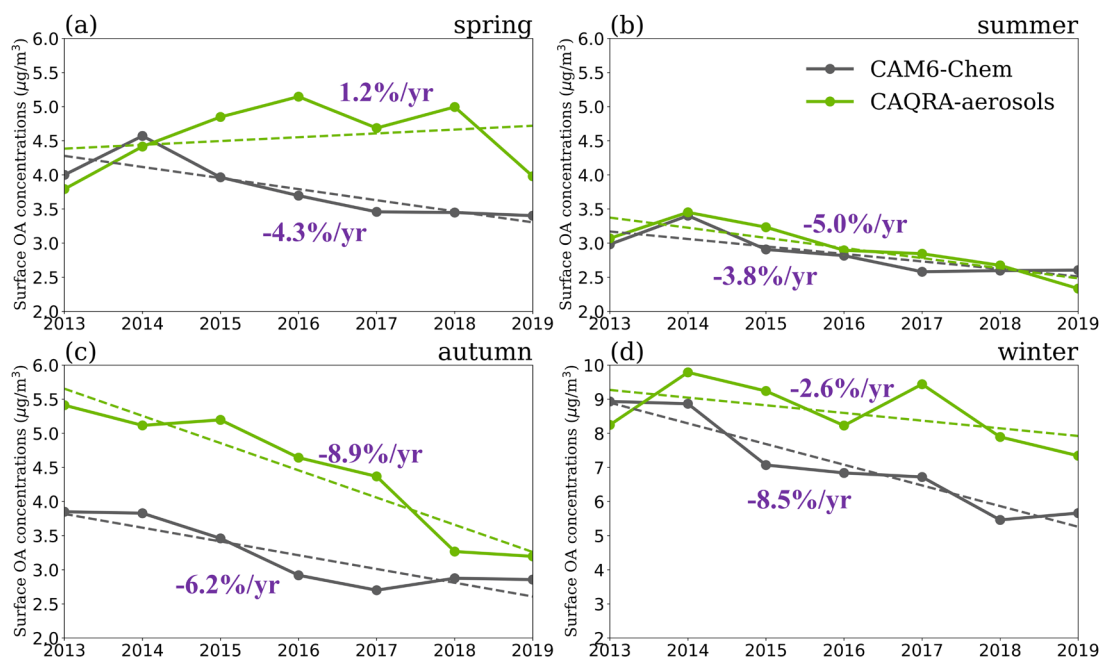
42 Figure S2. 2013 to 2019 annual average of surface organic aerosols (OA) concentrations in CAM6-Chem (a) and the CAQRA-
 aerosols dataset (b) (unit: $\mu\text{g m}^{-3}$).



44

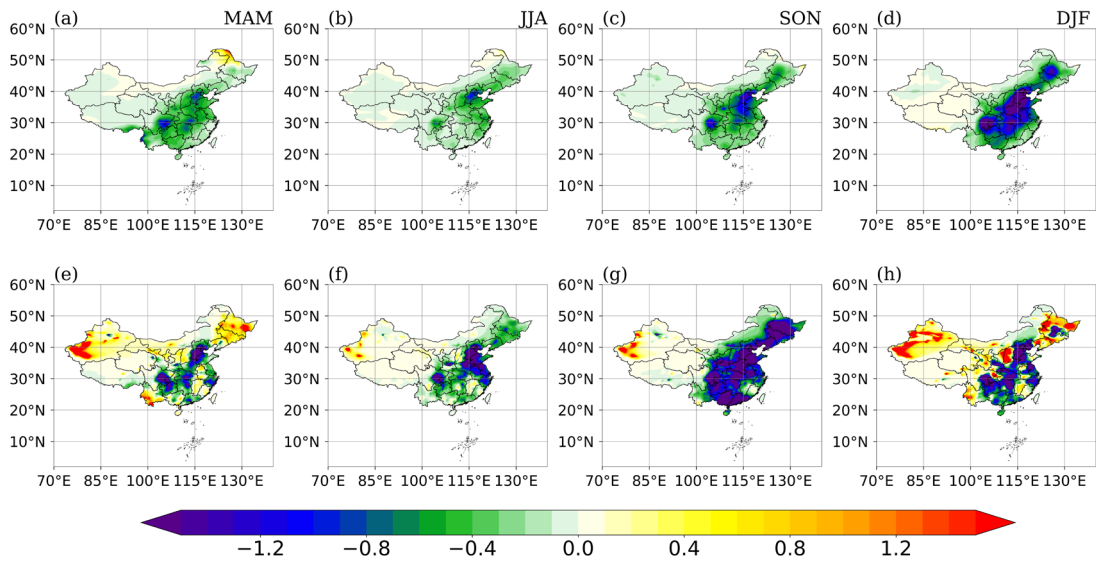
46

Figure S3. 2013 to 2019 MAM (first column), JJA (second column), SON (third column) and DJF (fourth column) average of surface organic aerosols (OA) concentrations in CAM6-Chem (first line) and the CAQRA-aerosols dataset (second line) (unit: $\mu\text{g m}^{-3}$).



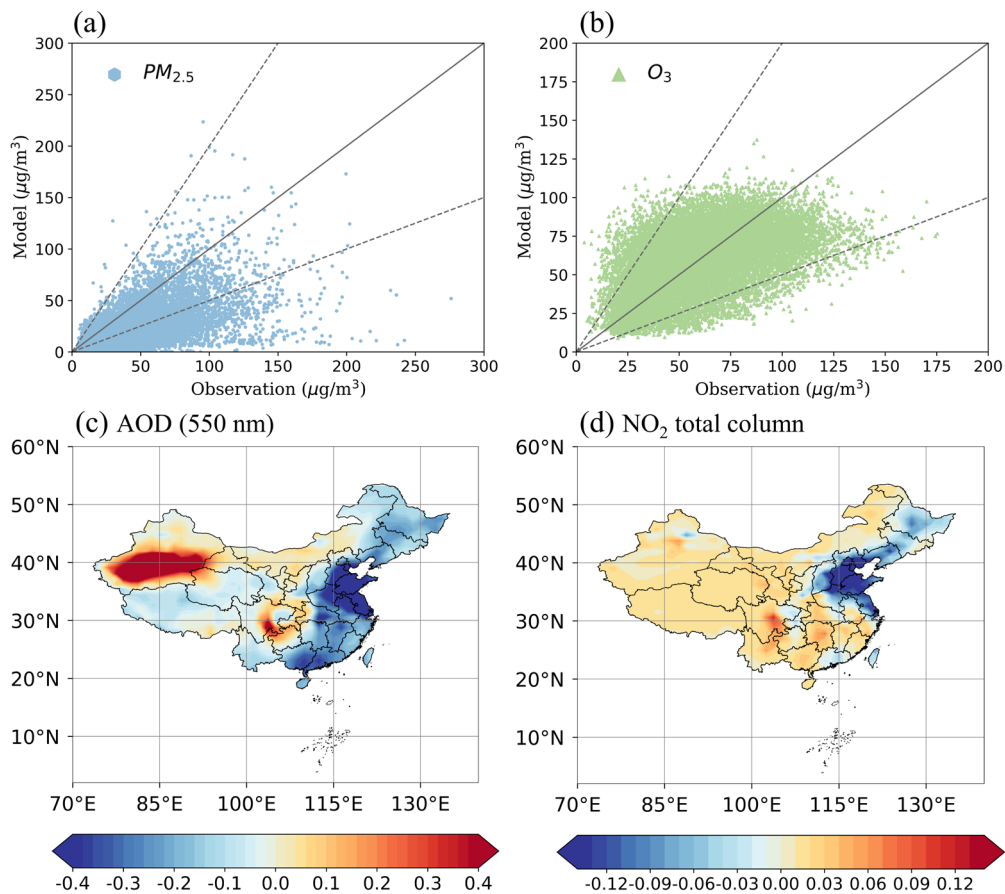
48

Figure S4. 2013 to 2019 interannual variation of different seasonal average surface organic aerosol (OA) concentrations in CAM6-Chem (dark grey) and the CAQRA-aerosols dataset (green) (unit: $\mu\text{g m}^{-3}$) and their trend lines (dotted line).



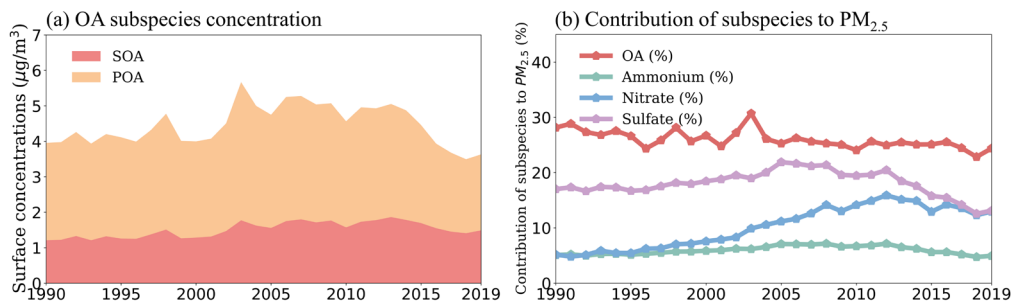
50

52 **Figure S5.** 2013 to 2019 MAM (first column), JJA (second column), SON (third column) and DJF (fourth column) average long-term trend of surface organic aerosols (OA) concentrations in CAM6-Chem (first line) and the CAQRA-aerosols dataset (second line) (unit: $\mu\text{g m}^{-3}$ per year).

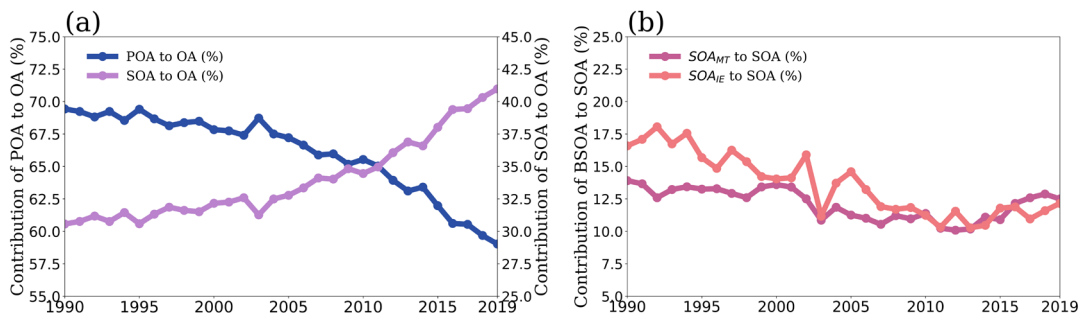


54

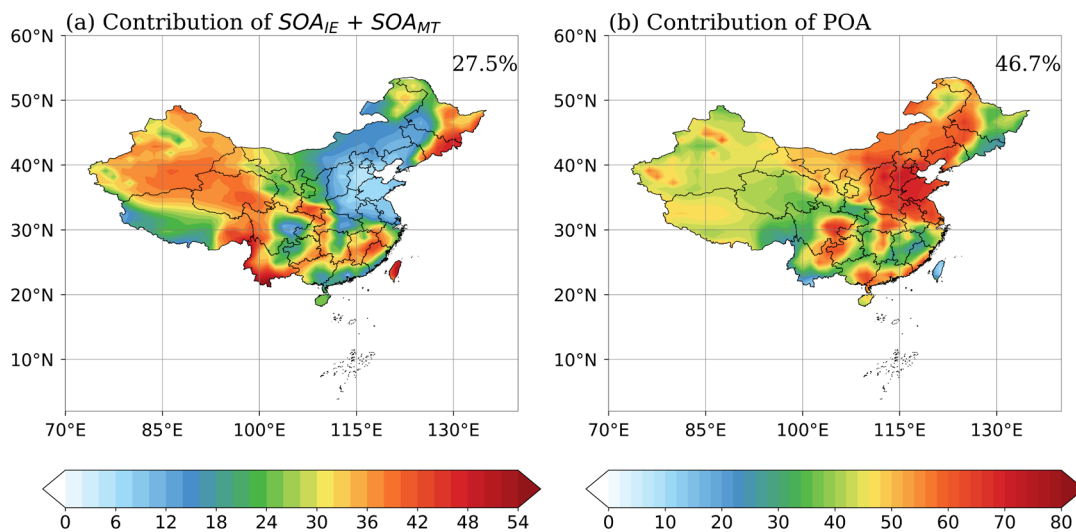
56 **Figure S6. Validation of modelled surface $PM_{2.5}$ (a) and O_3 (b) concentrations based on the National Urban Air Quality Real-Time**
 57 **Dissemination Platform of the China Environmental Monitoring General Station (unit: $\mu\text{g m}^{-3}$) from 2014 to 2019. The annual**
 58 **average climatological difference between the aerosol optical depth (AOD) (c) and the NO_2 column concentrations (d; unit: Tg)**
simulated by the model and satellite observations from 2000 to 2019.



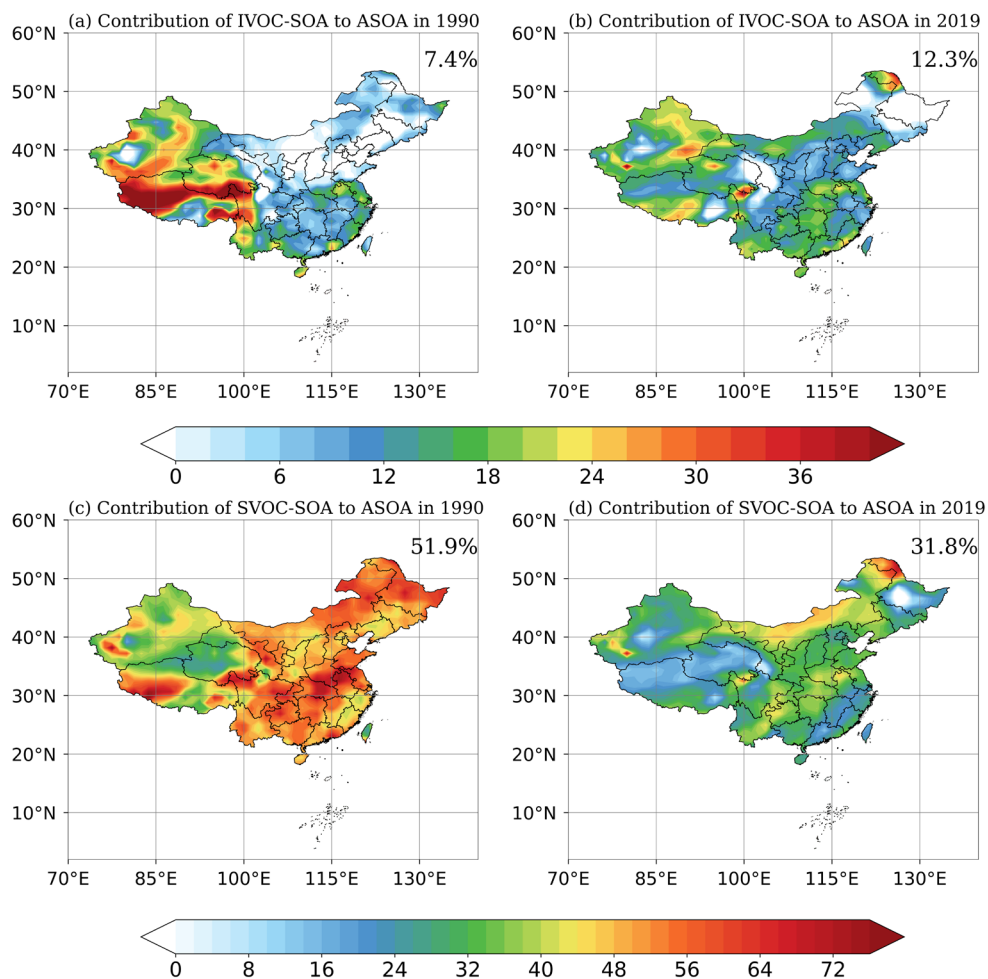
60 **Figure S7. (a) Interannual variations in modelled surface concentrations of organic aerosols (OA) subspecies primary organic**
 61 **aerosols (POA) and secondary organic aerosols (SOA) (unit: $\mu\text{g m}^{-3}$). (b) Interannual variations in the proportion of important**
 62 **components (OA, sulfate, nitrate, and ammonium) of $PM_{2.5}$ (unit: %).**



64 Figure S8. (a) Interannual variations in the contribution of subspecies primary organic aerosols (POA) and secondary organic aerosols (SOA) to organic aerosols (OA) (unit: %). (b) Interannual variations in the contribution of subspecies isoprene-epoxydiol-
 66 derived secondary organic aerosols (SOA_{IE}) and monoterpene-derived secondary organic aerosols (SOA_{MT}) to SOA (unit: %).

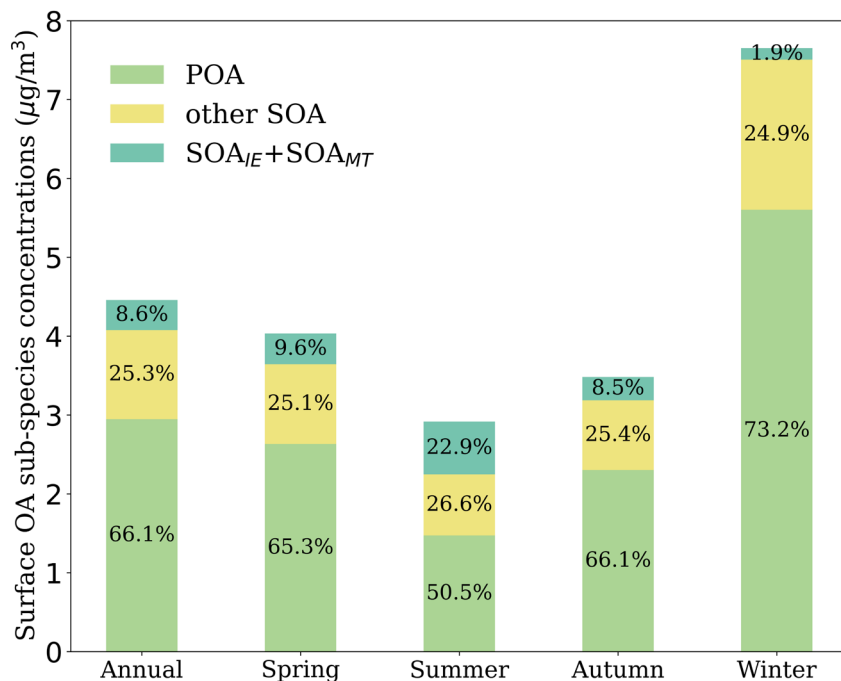


68 Figure S9. (a) 1990 to 2019 JJA average contribution of isoprene-epoxydiol-derived secondary organic aerosols + monoterpene-
 70 derived secondary organic aerosols (SOA_{IE} + SOA_{MT}) to organic aerosols (OA) (unit: %). (b) 1990 to 2019 JJA average contribution of primary organic aerosols (POA) to OA (unit: %). Spatial averages are shown in the upper right corner.



72 **Figure S10. (a-b) Contribution of secondary organic aerosols derived from intermediate-volatile organic compounds (IVOC-SOA) to secondary organic aerosols from anthropogenic sources (ASOA) in 1990 and 2019 (unit: %). (c-d) Contribution of secondary organic aerosols derived from semi-volatile organic compounds (SVOC-SOA) to secondary organic aerosols from anthropogenic sources (ASOA) in 1990 and 2019 (unit: %). Spatial averages are shown in the upper right corner.**

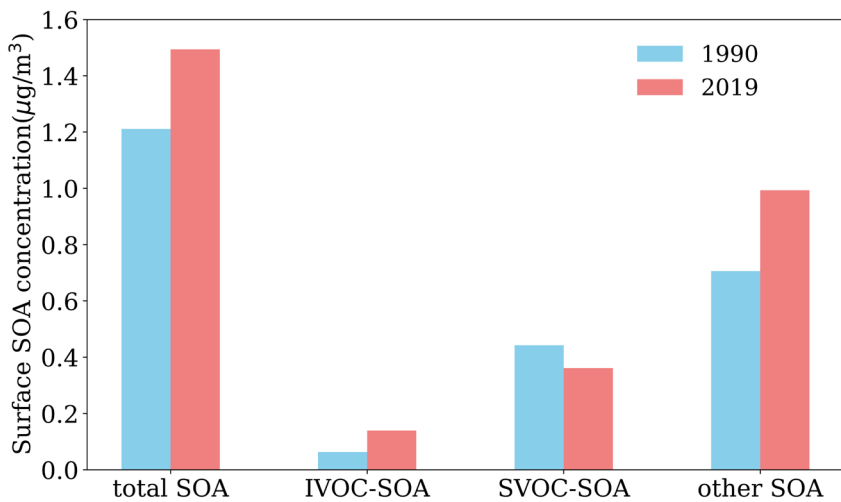
74



76

78

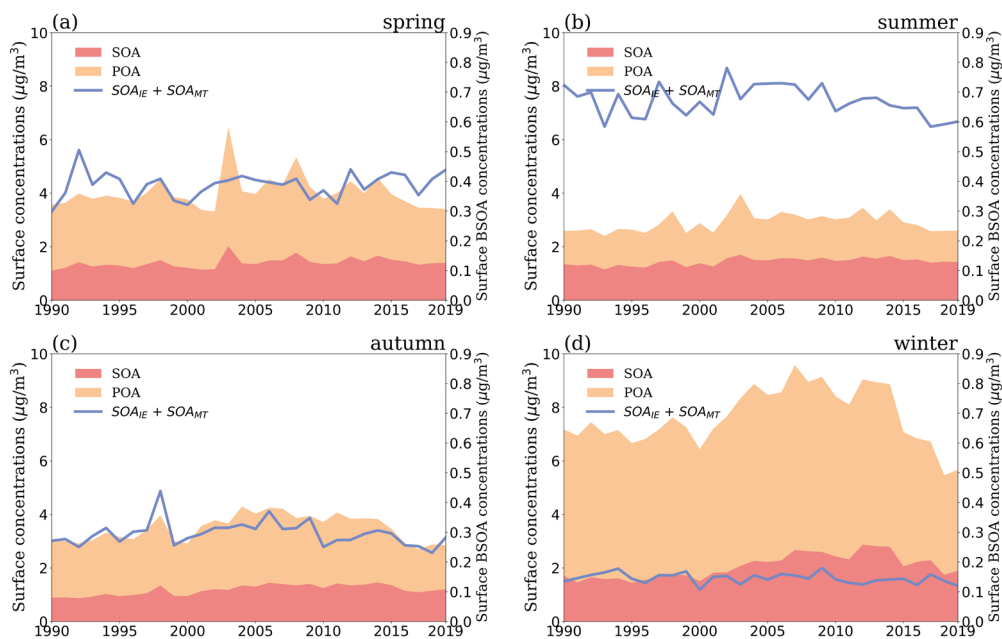
Figure S11. Annual and seasonal average contributions of organic aerosols (OA) subspecies primary organic aerosols (POA), isoprene-epoxydiol-derived secondary organic aerosols + monoterpene-derived secondary organic aerosols (SOA_{IE} + SOA_{MT}) and other secondary organic aerosols (SOA) to OA.



80

82

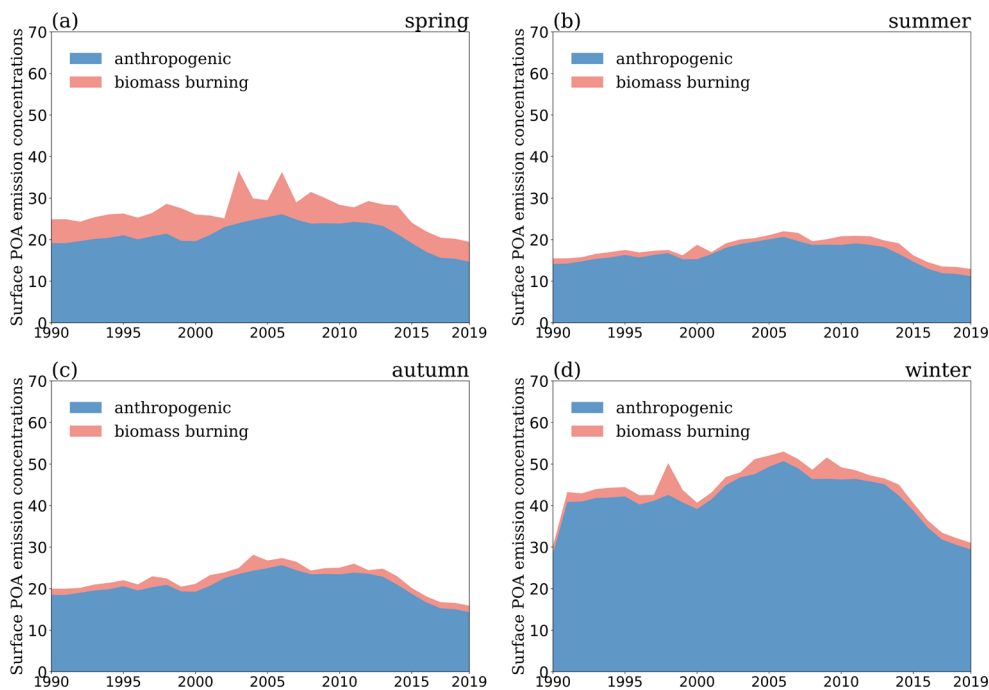
Figure S12. Annual surface secondary organic aerosols (SOA) concentrations (unit: $\mu\text{g m}^{-3}$) for total SOA, secondary organic aerosols derived from intermediate-volatile organic compounds (IVOC-SOA), secondary organic aerosols derived from semi-volatile organic compounds (SVOC-SOA), and other SOA in 1990 (blue) and 2019 (red).



84

86

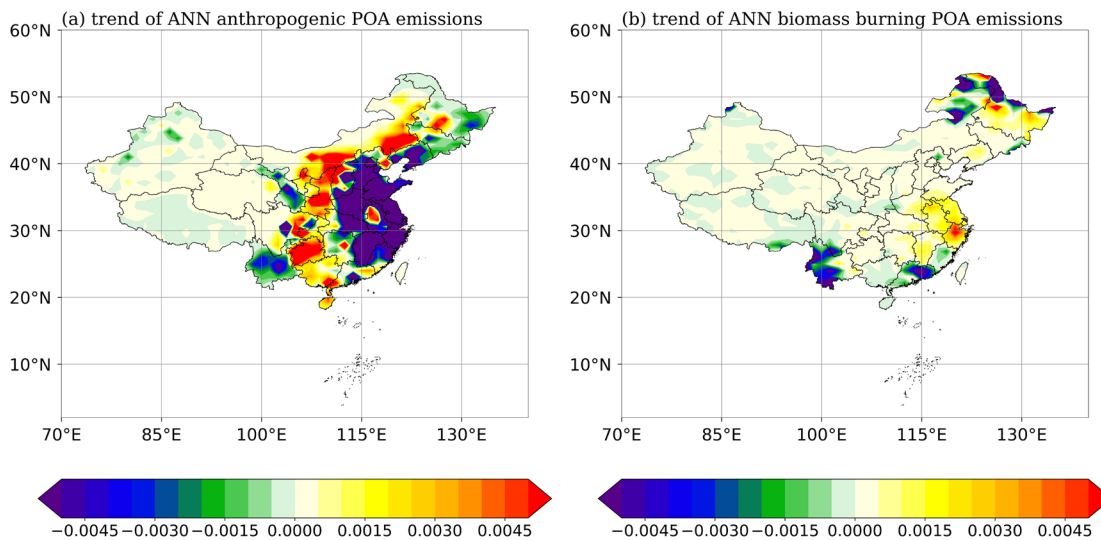
Figure S13. Seasonal average variation in modelled surface concentrations of organic aerosols (OA) subspecies primary organic aerosols (POA; left Y axis), secondary organic aerosols (SOA; left Y axis), isoprene-epoxydiol-derived secondary organic aerosols + monoterpene-derived secondary organic aerosols ($\text{SOA}_{\text{IE}} + \text{SOA}_{\text{MT}}$; right Y axis) (unit: $\mu\text{g m}^{-3}$).



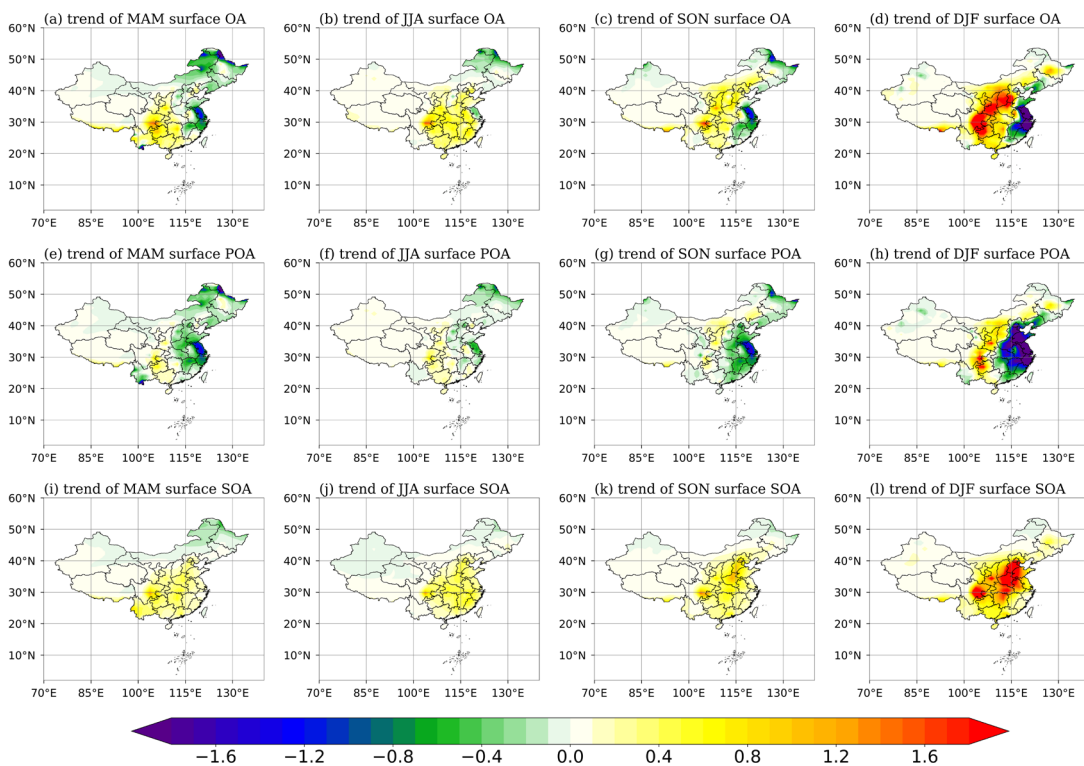
88

90

Figure S14. 1990 to 2019 seasonal average variation of surface anthropogenic (blue) and biomass burning (pink) primary organic aerosols (POA) emissions (unit: $\text{g m}^{-2} \text{mon}^{-1}$).

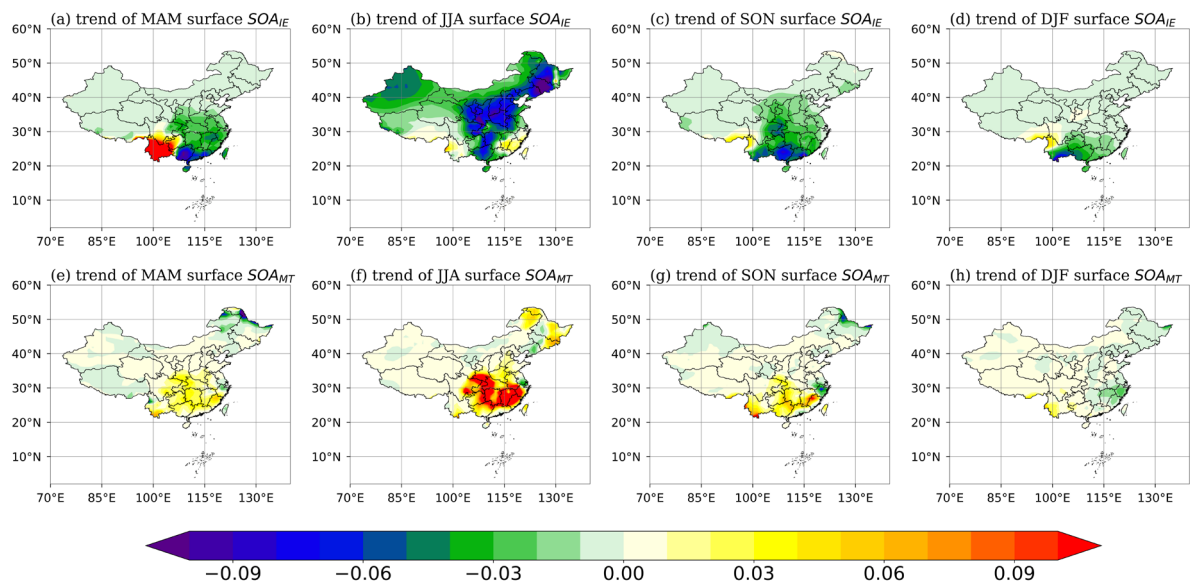


92 **Figure S15.** 1990 to 2019 annual average long-term trend of anthropogenic primary organic aerosols (POA) emissions (a; unit: g m^{-2} per decade) and biomass burning POA emissions (b; unit: g m^{-2} per decade).



94

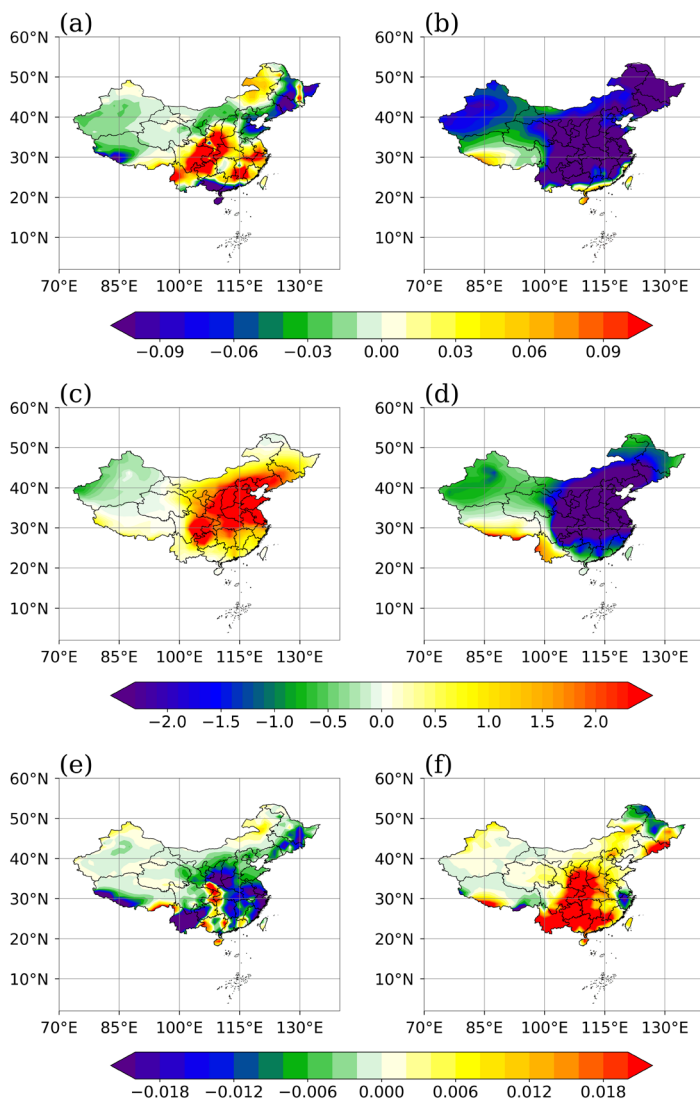
96 **Figure S16.** 1990 to 2019 MAM (first column), JJA (second column), SON (third column) and DJF (fourth column) average long-term trend of surface organic aerosols (OA; a-d) and its components primary organic aerosols (POA; e-h), secondary organic aerosols (SOA; i-l) concentrations (unit: $\mu\text{g m}^{-3}$ per decade).



98

100

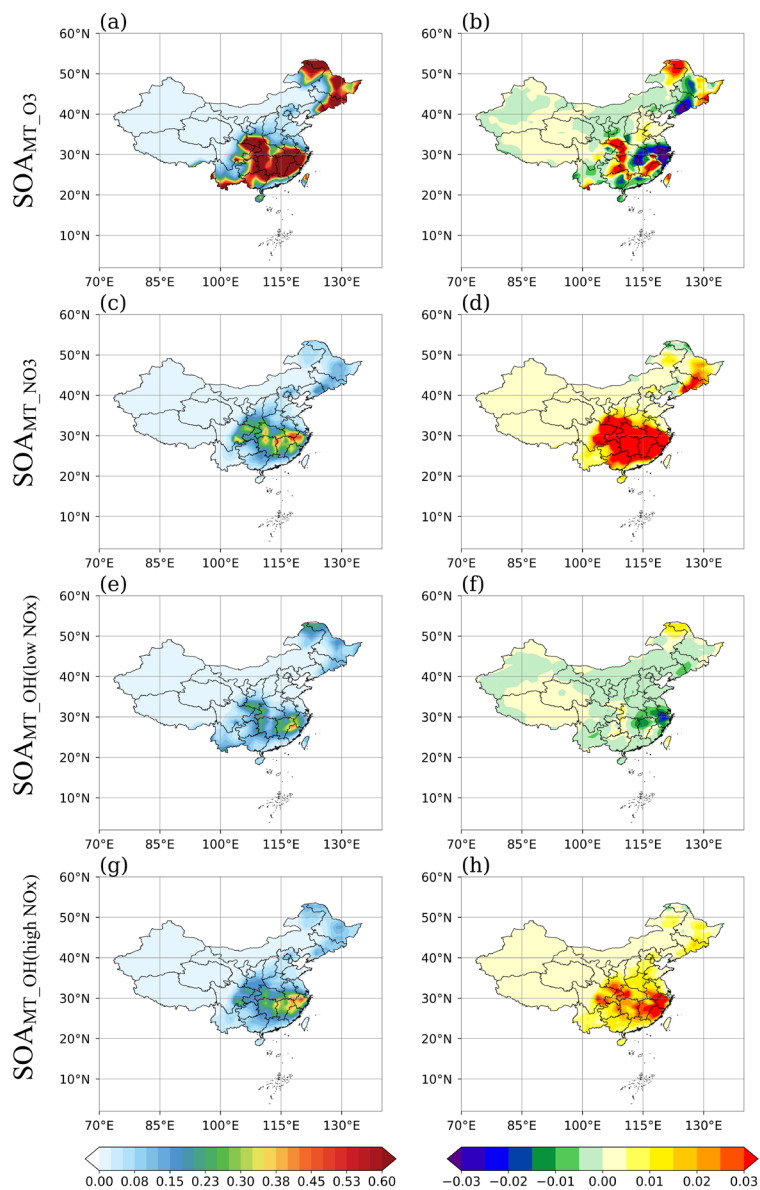
Figure S17. 1990 to 2019 MAM (first column), JJA (second column), SON (third column) and DJF (fourth column) average long-term trend of surface isoprene-epoxydiol-derived secondary organic aerosols (SOA_{IE} ; a-d) and monoterpene-derived secondary organic aerosols (SOA_{MT} ; e-h) concentrations (unit: $\mu\text{g m}^{-3}$ per decade).



102

104

Figure S18. The JJA average long-term trends of surface isoprene-epoxydiol-derived secondary organic aerosols (SOA_{IE}; a-b; unit: $\mu\text{g m}^{-3}$ per decade), organosulfate (SO₄²⁻; c-d; unit: $\mu\text{g m}^{-3}$ per decade), and isoprene epoxydiol (IEPOX; e-f; unit: ppb per decade) concentrations for the periods 1990-2006 (left column) and 2006-2019 (right column).

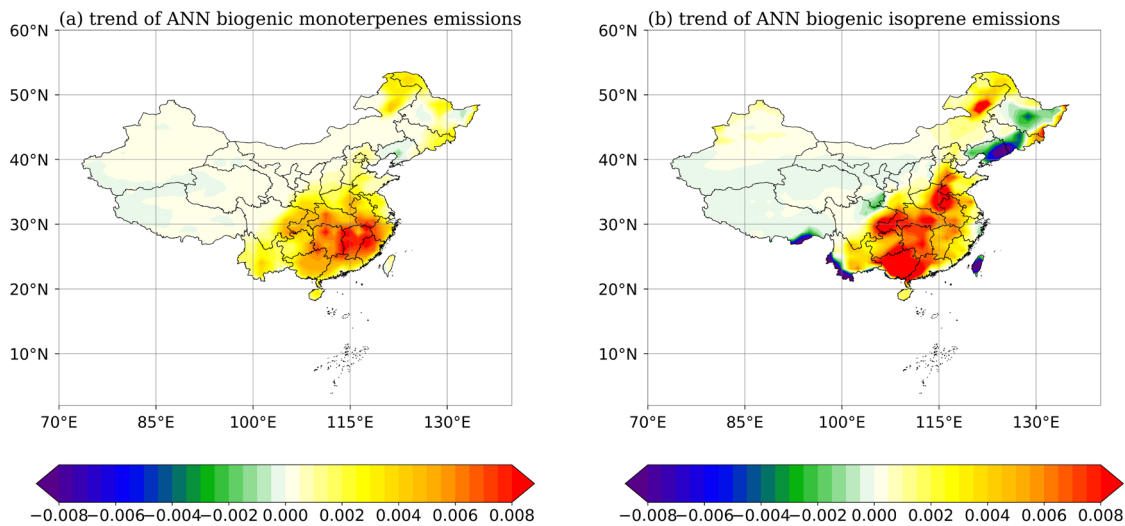


106

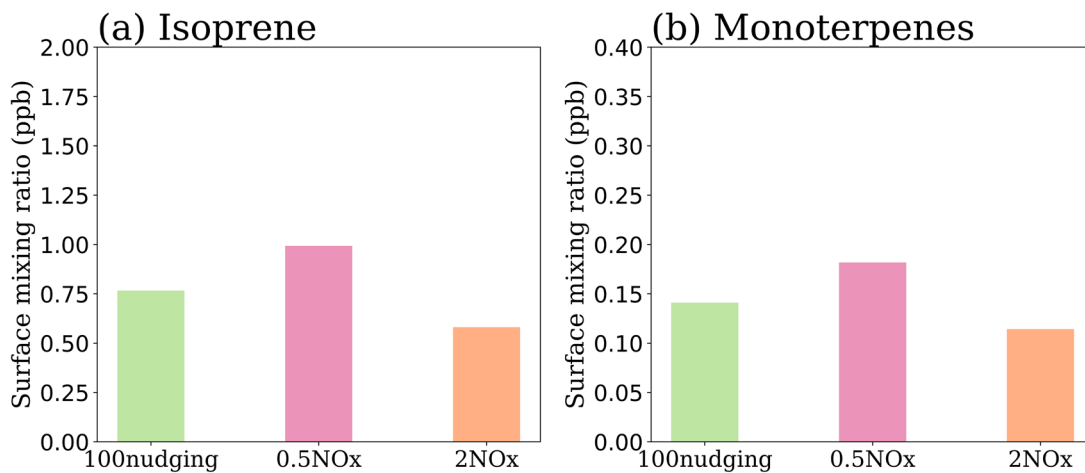
108

110

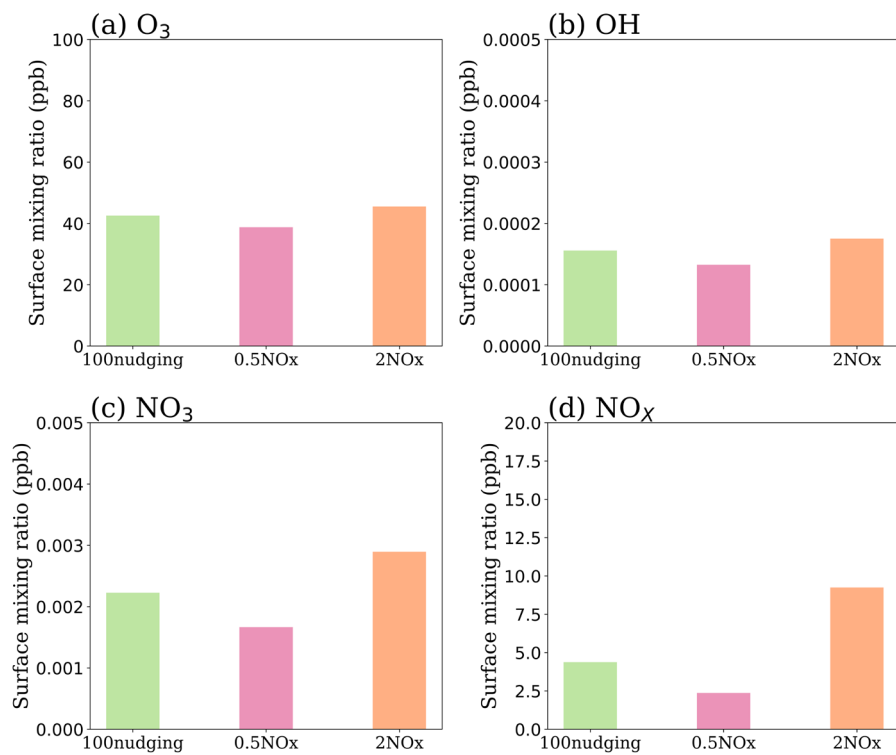
Figure S19. 1990 to 2019 JJA average (left column; unit: $\mu\text{g m}^{-3}$) and long-term trend (right column; unit: $\mu\text{g m}^{-3}$ per decade) of surface monoterpene-derived secondary organic aerosols (SOA_{MT}) oxidized by O₃ (SOA_{MT}_O₃; a-b), SOA_{MT} oxidized by NO₃ (SOA_{MT}_NO₃; c-d), SOA_{MT} oxidized by OH under low NO_x condition (SOA_{MT}_OH_(low NO_x); e-f) and SOA_{MT} oxidized by OH under high NO_x condition (SOA_{MT}_OH_(high NO_x); g-h) concentrations.



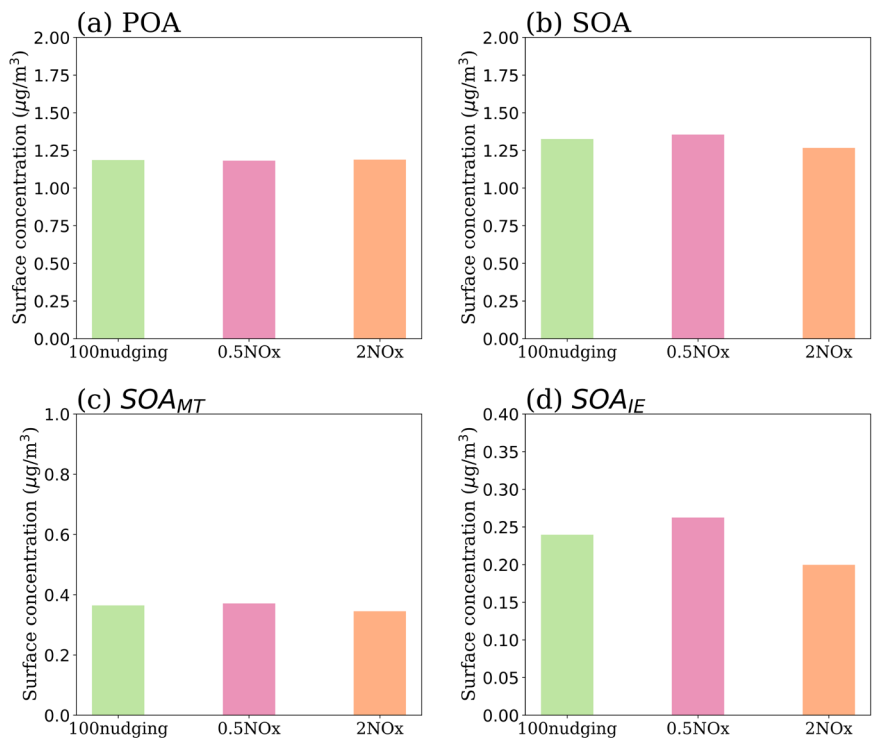
112 **Figure S20. 1990 to 2019 annual average long-term trend of biogenic monoterpene emissions (a) and biogenic isoprene emissions (b) (unit: g m^{-2} per decade).**



114 **Figure S21. Surface concentrations (unit: ppb) of (a) isoprene and (b) monoterpenes for July 2013 from the NOx sensitivity**
 116 **experiments named 100nudging (green bar), 0.5NOx (pink bar) and 2NOx (orange bar).**



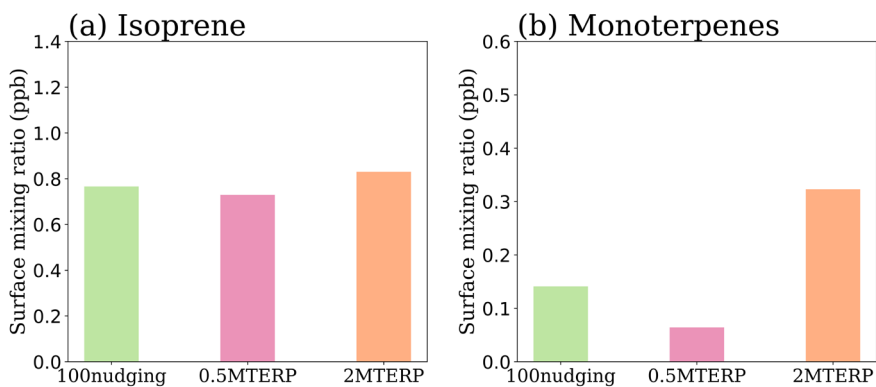
118 **Figure S22.** Surface concentrations (unit: ppb) of (a) O₃, (b) OH, (c) NO₃ and (d) NO_x for July 2013 from the NO_x sensitivity experiments named 100nudging (green bar), 0.5NO_x (pink bar) and 2NO_x (orange bar).



120

Figure S23. Surface concentrations (unit: $\mu\text{g m}^{-3}$) of primary organic aerosols (POA; a), secondary organic aerosols (SOA; b), monoterpene-derived secondary organic aerosols (SOA_{MT} ; c), isoprene-epoxydiol-derived secondary organic aerosols (SOA_{IE} ; d) for July 2013 from the NOx sensitivity experiments named 100nudging (green bar), 0.5NOx (pink bar) and 2NOx (orange bar).

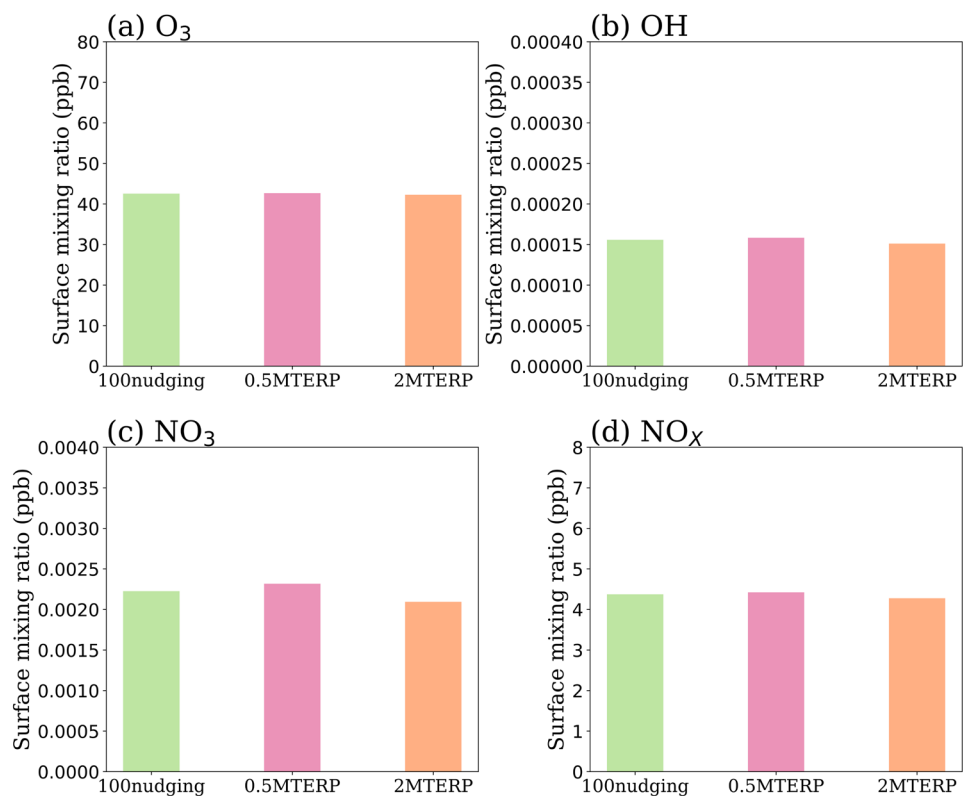
122



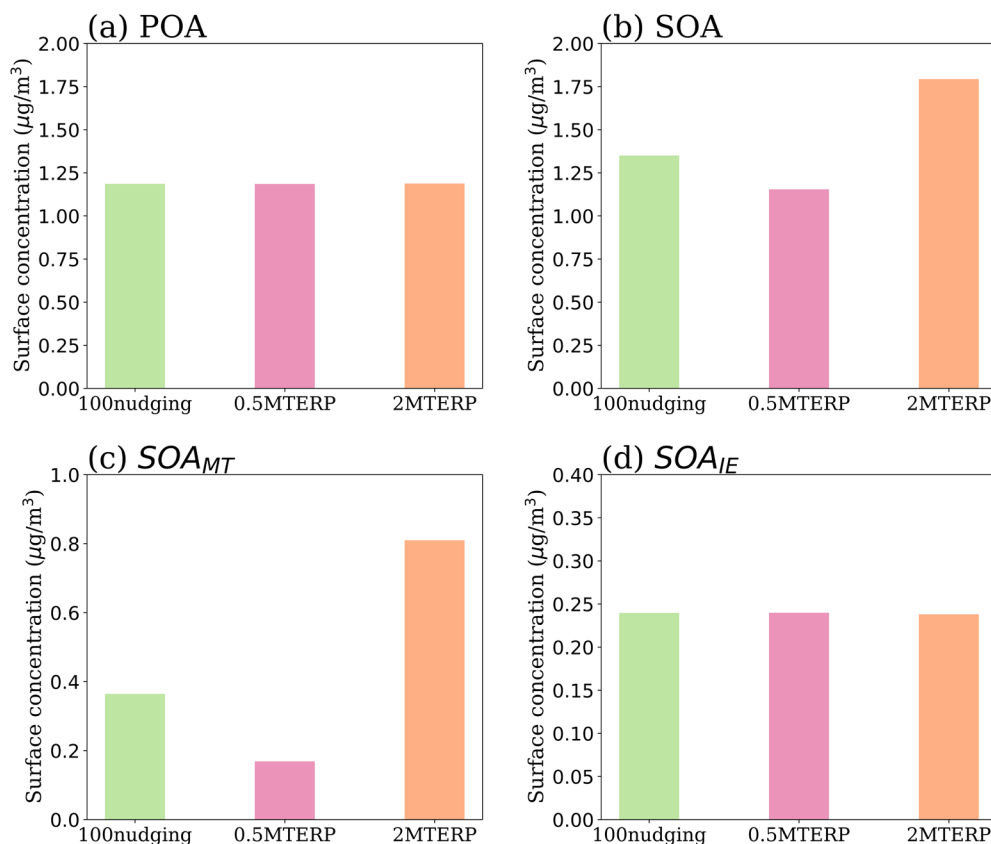
124

Figure S24. Surface concentrations (unit: ppb) of (a) isoprene and (b) monoterpenes for July 2013 from the monoterpenes sensitivity experiments named 100nudging (green bar), 0.5MTERP (pink bar), and 2MTERP (orange bar).

126



128 **Figure S25. Surface concentrations (unit: ppb) of (a) O₃, (b) OH, (c) NO₃ and (d) NO_x for July 2013 from the monoterpenes sensitivity experiments named 100nudging (green bar), 0.5MTERP (pink bar), and 2MTERP (orange bar).**



130 **Figure S26. Surface concentrations (unit: $\mu\text{g m}^{-3}$) of primary organic aerosols (POA; a), secondary organic aerosols (SOA; b),**
 132 **monoterpene-derived secondary organic aerosols (SOA_{MT} ; c), isoprene-epoxydiol-derived secondary organic aerosols (SOA_{IE} ; d) for**
 134 **July 2013 from the monoterpenes sensitivity experiments named 100nudging (green bar), 0.5MTERP (pink bar), and 2MTERP**
(orange bar).

References

- 136 Emmons, L. K., Schwantes, R. H., Orlando, J. J., Tyndall, G., Kinnison, D., Lamarque, J., Marsh, D., Mills, M. J., Tilmes, S.,
 Bardeen, C., Buchholz, R. R., Conley, A., Gettelman, A., Garcia, R., Simpson, I., Blake, D. R., Meinardi, S., and Pétron, G.:
 138 The Chemistry Mechanism in the Community Earth System Model Version 2 (CESM2), *J Adv Model Earth Syst*, 12,
 e2019MS001882, <https://doi.org/10.1029/2019MS001882>, 2020.
- 140 Jo, D. S., Hodzic, A., Emmons, L. K., Tilmes, S., Schwantes, R. H., Mills, M. J., Campuzano-Jost, P., Hu, W., Zaveri, R. A.,
 Easter, R. C., Singh, B., Lu, Z., Schulz, C., Schneider, J., Shilling, J. E., Wisthaler, A., and Jimenez, J. L.: Future changes in
 142 isoprene-epoxydiol-derived secondary organic aerosol (IEPOX SOA) under the Shared Socioeconomic Pathways: the
 importance of physicochemical dependency, *Atmos. Chem. Phys.*, 21, 3395–3425, <https://doi.org/10.5194/acp-21-3395-2021>,
 144 2021.

Schwantes, R. H., Emmons, L. K., Orlando, J. J., Barth, M. C., Tyndall, G. S., Hall, S. R., Ullmann, K., St. Clair, J. M., Blake,
146 D. R., Wisthaler, A., and Bui, T. P. V.: Comprehensive isoprene and terpene gas-phase chemistry improves simulated surface
ozone in the southeastern US, *Atmos. Chem. Phys.*, 20, 3739–3776, <https://doi.org/10.5194/acp-20-3739-2020>, 2020.

148 Tilmes, S., Hodzic, A., Emmons, L. K., Mills, M. J., Gettelman, A., Kinnison, D. E., Park, M., Lamarque, J. -F., Vitt, F.,
Shrivastava, M., Campuzano-Jost, P., Jimenez, J. L., and Liu, X.: Climate Forcing and Trends of Organic Aerosols in the
150 Community Earth System Model (CESM2), *J. Adv. Model. Earth Syst.*, 11, 4323–4351,
<https://doi.org/10.1029/2019MS001827>, 2019.

152